PAPER • OPEN ACCESS

Particle transport in reduced turbulence neutral beam heated discharges at Wendelstein 7-X

OPEN ACCESS
IOP Publishing | International Atomic Energy Agency
Nuclear Fusion
Nucl. Fusion **64** (2024) 106015 (13pp)
https://doi.org/10.1088/1741-4326/ad6b37

Particle transport in reduced turbulence neutral beam heated discharges at Wendelstein 7-X

S. Bannmann*, O. Ford, P.Zs. Poloskei, J. Svensson, A. Pavone, S. Kwak, U. Hoefel, E. Pasch, G. Fuchert, H.M. Smith, S. Lazerson, P. McNeely, N. Rust, D. Hartmann, R.C. Wolf and the W7-X Team[a]

Max-Planck-Institut für Plasmaphysik, Wendelsteinstr. 1, 17491 Greifswald, Germany

E-mail: sebastian.bannmann@ipp.mpg.de

Received 26 April 2024, revised 15 July 2024
Accepted for publication 4 August 2024
Published 22 August 2024

Abstract

A spontaneous reduction in anomalous particle transport in the plasma core is seen experimentally in reproducible, purely neutral beam heated plasma phases at Wendelstein 7-X (W7-X). Heating and fueling the plasma exclusively with the neutral beam injection system for several seconds leads to continuously peaking plasma density profiles with strong gradients inside mid minor radius. A significant acceleration of the density peaking occurs after a certain onset time and is examined with a detailed particle transport analysis in several discharges. By invoking the particle continuity equation, the total experimental radial electron flux is deduced from the time evolution of the electron density profile and the radially resolved particle sources. Subtracting the modeled neoclassical particle flux contribution gives the anomalous particle flux. Exploiting the evolving plasma conditions, anomalous diffusion and convection coefficients are computed from the flux variation with density and density gradients. In several discharges a significant and consistent change of the anomalous transport coefficients is seen when crossing a specific normalized density gradient length.

Keywords: particle transport, neutral beam heated plasma, Wendelstein 7-X, stellarator

(Some figures may appear in colour only in the online journal)

1. Introduction

Wendelstein 7-X is a magnetic confinement fusion experiment of the stellarator type [1, 2] where the magnetic field topology was optimized to, among other goals, reduce the neoclassical heat and particle losses of electrons and main plasma ions. The success of the neoclassical optimization regarding the energy transport could be demonstrated experimentally in some pellet fueled discharges [3]. Nevertheless, gas fueled electron cyclotron resonance (ECR) heated plasmas at W7-X exhibit much higher heat transport levels than the neoclassical predictions. The strong transport is attributed to turbulent processes caused by modes such as the ITG mode [4, 5]. High performance, reduced turbulence plasmas reaching a significantly higher core ion temperature were achieved in the presence of peaked density profiles which lead to a stabilization of the ion scale turbulence [6, 7]. The density peaking in these discharges was reached transiently by pellet injection, i.e. by the introduction of a central particle source. At W7-X, peaked density profiles also occur in purely neutral beam injection (NBI) heated plasma phases, possibly opening up an alternative route to high

[a] See Grulke *et al* 2024 (https://doi.org/10.1088/1741-4326/ad2f4d) for the W7-X Team.
* Author to whom any correspondence should be addressed.

performance plasmas. Studying and controlling such plasmas requires an understanding of the particle transport under such conditions. The scope of this paper is to analyze the radial electron and main ion particle transport in non steady state NBI heated plasmas from an experimental point of view using plasma profile data from the Thomson scattering system and the CXRS system together with modeled particle sources. It is shown in the results section 3 by applying the methodology described in section 2 that a spontaneous change of density peaking behavior seen in several discharges is connected to a non-transient change in anomalous transport. In the analyzed discharges, a strong impurity accumulation was observed and attributed to a reduction of the transport to neoclassical levels which is shown in [8].

In stellarators, in the presence of temperature gradients neoclassical particle transport can lead to hollow density profiles if there is no strong central particle source [9]. Under the assumption of dominant neoclassical transport this was predicted for W7-X experimental conditions [10]. As hollow density profiles are not seen experimentally, strong anomalous particle transport must be prevalent in W7-X. A first numerical study indeed concluded that in ECR heated plasmas, which exhibit strong electron temperature gradients, an anomalous inward particle flux exists, leading to the observed flat density profiles and matching at least in sign the reconstructed experimental particle fluxes [11]. An analytical study showed that in the electrostatic and collisionless approximation the total quasilinear particle flux due to turbulent processes is directed outwards in quasi-isodynamic stellarators if there are no strong temperature gradients [12]. At W7-X, improved energy confinement states with temperature pedestals were seen and found to be dependent on the magnetic configuration [13]. At the preceding experiment, W7-AS, particle transport coefficients were determined from modulation experiments [14] and an anomalous particle pinch was found in plasmas with peaked density profiles [15]. At CHS, a similar analysis path as in this study was taken to calculate experimental electron transport coefficients from the full particle balance and determined a negative convection coefficient in the outer half of the plasma radius [16]. An overview of the experimental results of particle transport studies in LHD is given in [17]. One of the results is that at an electron temperature of 1.25 keV the experimentally determined outward particle convection is smaller than calculated from neoclassical theory, indicating the presence of an additional, anomalous inward convection. In tokamaks, the particle diffusion and convection have significant anomalous contributions [18] and e.g. ITG and TEM turbulence modifies the observed pinch velocity [19].

2. Methods

The most important quantities when studying the particle transport in a magnetic confined plasma are the radial particle fluxes of electrons and main ions. As there are no diagnostics available providing a direct measurement of radial fluxes, experimentally, it is necessary to compute these indirectly from the global particle balance. Invoking the particle continuity equation, one can compute the total radial (anomalous + neoclassical + classical) particle flux of a given species through a flux surface $\rho = \frac{r}{a}$ as:

$$\Phi\left(r\right) = \int \left(S - \partial_t n\right) \mathrm{d}V \tag{2.1}$$

where S is the particle source term, $\partial_t n$ is the time derivative of the density and the integral is performed over the volume enclosed by the flux surface. Due to the fast transport processes along the magnetic field lines it is justified to assume the plasma density to be equal everywhere on a flux surface. There is no reason on the other hand for the radial particle fluxes to be equal at every point on a flux surface as the transport processes depend on local magnetic field properties and real space plasma parameter gradients. Consequently, the flux computed by 2.1 has to be interpreted as the flux surface averaged value. As the plasma phases to be analyzed do not have any significant hydrogen gas puffing, the only particle source terms to be considered are recycling hydrogen from the divertor and first wall and hydrogen injected with the neutral beam system. Thus, equation (2.1) can be written as:

$$\Gamma\left(r\right) = \left(\frac{\mathrm{d}V}{\mathrm{d}r}\right)^{-1} \int_0^r \left(S_{\mathrm{NBI}} + S_{\mathrm{RCY}} - \partial_t n\right) \frac{\mathrm{d}V}{\mathrm{d}r'} \mathrm{d}r' \tag{2.2}$$

where $\frac{\mathrm{d}V}{\mathrm{d}r}$ is the flux surface area, S_{NBI} the NBI particle source, S_{RCY} the particle source due to recycling hydrogen, $\partial_t n$ the time derivative of the plasma density and V the volume enclosed by a flux surface. The radial particle flux density Γ can be split into well known classical and neoclassical contributions and an anomalous contribution caused by turbulent processes:

$$\Gamma \quad = \quad \Gamma_{\mathrm{CL}} + \Gamma_{\mathrm{NC}} + \Gamma_{\mathrm{anom}}. \tag{2.3}$$

The anomalous flux is assumed to be ambipolar and commonly parameterized using a diffusion and a convection coefficient (compare e.g. [20, 21]):

$$\Gamma_{\mathrm{anom}} = -D_A \nabla n + V_A n. \tag{2.4}$$

To compute the radial particle flux and its anomalous contribution the particle source terms, the time evolution of the plasma density profile and the neoclassical flux need to be determined.

2.1. Particle source—NBI

The NBI system at W7-X is capable of injecting neutral hydrogen with an energy of up to $E_{\mathrm{inj}} = 55$ keV and a power injected into the torus of up to $P_{\mathrm{NBI}} \approx 1.8$ MW per source [22, 23]. In operation phase 1.2B, on which this analysis focuses, 2 out of 8 sources (S7, S8) were operated. At full power the total number of particles injected into the plasma is approximately $5.2 \times 10^{20}\ \mathrm{s}^{-1}$. The ionization rate depends on both the density

profile and the beam geometry and so varies along the beam path through the plasma. To model the beam particle deposition profile a verified forward model based on Gaussian pencil beams is used, which is described in detail in [24]. The beam model provides 3D spatial density distributions $n_b^{(i)}(\vec{x})$ of beam neutrals in the first 6 hydrogen energy states i. The local particle source rate S is then computed as:

$$S(\vec{x}) = V_{\text{cell}} \sum_{i=1}^{6} n_b^{(i)} n_e \left(\left\langle \sigma_e^{(iI)} v \right\rangle + \left\langle \sigma_p^{(iI)} v \right\rangle \right) \tag{2.5}$$

where V_{cell} is the local cell volume and $\langle \sigma^{(iI)} v \rangle$ are the Maxwell averaged cross sections of electron and ion impact ionization processes respectively. Additionally, a significant fraction of beam neutrals are ionized by charge exchange (CX) reactions with plasma ions. However, this does not lead to a local increase of the plasma density but creates a new neutral species the halo. The halo neutrals can undergo several CX reactions before finally being ionized by electron or ion collisions. The employed model includes this effect on the particle deposition profile by carefully modeling the halo cloud forming around the beam. As shown in [24] an appreciable effect is to be expected only in low density plasmas. Apart from the plasma density profile the particle deposition profile depends on the beam injection power, the beam species fractions and the beam shape (divergence, positioning in space). To improve the accuracy of the model these parameters were explicitly fitted for the analyzed discharges using beam emission spectroscopy data.

2.2. Particle source—recycling

Only a small fraction of the hydrogen ions leaving the plasma through the last closed flux surface (LCFS) are pumped out of the plasma vessel. The larger fraction of particles will reenter the plasma volume after neutralization in the divertor or first wall region. Thereby, hydrogen particles undergo many cycles through the plasma before they are finally removed from the system. To model the particle source rate due to these recycling neutral fluxes a strongly simplified 1D model is implemented. It assumes a homogeneous influx of neutrals over the whole LCFS thereby eliminating any spatial dependencies on the toroidal or poloidal angle. If estimating the recycling flux to match the total plasma particle loss at each time point, the magnitude of the influx can be written in terms of the global plasma particle confinement time and the total plasma particle content:

$$\Phi_{\text{RCY}} = \frac{\int n_e \mathrm{d}V}{\tau_p}. \tag{2.6}$$

The recycling flux arriving at the LCFS is assumed to have the same temperature as the surrounding plasma. When penetrating the plasma the neutrals are rapidly ionized by electron and ion impact collisions as well as CX reactions with plasma ions. CX reactions do not lead to a local plasma fueling but lead to a much deeper penetration depth of neutrals into the plasma core. To correctly model the resulting neutral density profile in the confined region, a CX diffusion equation is solved tracking several excited hydrogen states and taking the initial CX reactions of the recycling particles with the plasma as the source term. The implemented model is analogous to the CX diffusion model of the beam halo described in [24] and is written in compact form as:

$$-\nabla \left(D_{\text{CX}}^{(i)} \nabla n^{(i)} \right) = \sum_j T_{\text{CR}}^{(ij)} n^{(j)} + S^{(i)} \tag{2.7}$$

where $D_{\text{CX}}^{(i)}$ is the CX diffusion coefficient, $n^{(i)}$ the recycling neutral density and $S^{(i)}$ the direct CX source term of energy state i. The CX diffusion coefficient for thermal neutrals in energy state i is computed as (compare [24]):

$$D_{\text{CX}}^{(i)} = \frac{v_{\text{th}}^2}{2 n_{\text{i}} \sum_{j=1}^{j_{\max}} \left\langle \sigma_{CX}^{(i \to j)} v_r \right\rangle} \tag{2.8}$$

where n_i is the main ion density, v_{th} the thermal velocity, σ_{CX} the CX cross section and v_r the relative velocity. The matrix T_{CR} contains the collisional-radiative rates between all states. The upper triangle consists of the Einstein coefficients describing state depopulation due to photon emission. The lower triangle is filled with the reaction rates to higher states due to electron impact, ion impact and CX processes. The diagonal contains the summed loss rates to each state. The system of coupled diffusion equations is solved numerically enforcing a vanishing profile gradient on the axis and the total particle fueling to be equal to the loss rate as boundary conditions. After obtaining a recycling neutral density profile, equation (2.5) can be used to calculate the source rate (replacing n_b with the recycling neutral density). The particle confinement time of $\tau_p = (0.27 \pm 0.1) s$ used in the following analysis was determined in an independent global particle study [25]. The comparison of the model to neutral density estimations from Balmer-α emission data and a neutral particle transport calculation performed with EMC3-EIRENE in [26] is shown in the appendix in figure 10. The presented 1D recycling model agrees inside error bars with the data points from the spectroscopy measurements over the whole plasma radius and agrees well in the plasma core with the lower neutral density bound found by the EMC3-EIRENE calculation. As the recycling flux is higher in the divertor region than from the rest of the wall the resulting neutral density distribution is expected to be poloidally and toroidally asymmetric, which is not covered with the presented 1D CX diffusion model. This makes comparisons of the neutral density to experimental data measured at a certain position in the machine approximate. However, for modeling the total particle fueling of the plasma, knowledge of the exact poloidal and toroidal distribution is not necessary if using a model which is based on an independently determined particle confinement time.

2.3. Plasma profiles

The standard electron density profile diagnostic at W7-X is a Thomson scattering system consisting of 3 Nd:YAG lasers and two optical heads collecting the scattered laser light [27, 28]. The system has ≈30 individual measuring volumes across the minor plasma radius and from each measurement the local electron density and temperature can be reconstructed. Each laser has a repetition rate of 10 Hz which determines the time resolution of the measured profiles. The plasma ion temperature is measured with the CX recombination spectroscopy (CXRS) system [29]. Profile fits are computed from the raw data points using a Monte Carlo sampled local regression method with a window size of $\frac{\Delta r}{a} = 0.1$. The Thomson and CXRS data are averaged over a time window of 140 ms and 100 ms respectively.

2.4. Neoclassical transport

The neoclassical transport is not intrinsically ambipolar as the electrons and ions are in different collisionality regimes. A radial electric field must exist to equalize the electron and ion fluxes. Purely NBI heated plasmas at W7-X are typically in the so called ion-root regime with a negative (inward pointing) radial electric field over the whole plasma radius [30, 31]. The neoclassical and classical particle fluxes are computed using Neotransp [32] which finds a consistent solution of the radial electric field and particle fluxes fulfilling the ambipolarity condition for a given equilibrium and given plasma profiles. The library uses a database containing precomputed output of the drift kinetic equation solver (DKES) code. The impurity content of the plasma influences the neoclassical electron and main ion fluxes and vice versa. Assuming carbon to be the dominant core impurity species and varying Z_{eff} (effective charge) from 1.0 to 1.2, which covers the experimentally seen range for the analyzed discharges, leads to a variation of the neoclassical main ion fluxes of up to 20% depending on the radial position. Based on carbon density measurements in the plasma core ([33, 34] and compare appendix figure 9) $Z_{\mathrm{eff}} = 1.1 \pm 0.05$ is used in the following analysis. This value is in agreement with results from the Bremsstrahlung diagnostic [35].

3. Results

3.1. Particle flux analysis—discharge 20181009.034

All the steps necessary to deduce main ion particle fluxes from experimental density profiles and modeled particle sources are shown in detail in this chapter for a single discharge (20181009.034). An overview of the experimental program is shown in figure 1. During the plasma start-up phase from 0 s to 1 s the plasma is purely ECR heated (blue line) and actively fueled by the neutral gas inlet system (grey line). From 1 s to 3 s the plasma is purely NBI heated by two active sources (S7+S8) with a total injected power of $P \approx 3.7$ MW (green line). During the NBI phase the plasma density is rising as can be seen from the line integrated interferometer data (black line). The density rise is seen as a core density peaking which is clearly visible when looking at the core (orange line) and edge (light blue line) electron density measured by the Thomson system. The following transport analysis will focus on the plasma phase from 1.2 s to 3.0 s with a time resolution of 0.1 s.

3.1.1. Plasma profiles and particle sources. The plasma profiles of interest in the analyzed time interval are shown in figure 2. In the first (second/third) column the electron density (electron temperature/ion temperature) profile is plotted over the normalized radius (top) and over time at selected radii (bottom). During the pure NBI heated phase (1–3 s) the density keeps increasing inside mid radius and stays roughly constant in the outer half of the plasma, which is equivalent to the statement that the peaking increases. The strongest gradients build up between $r/a \approx 0.3$ to 0.4. Plots of the profile gradients and time derivatives can be found in the appendix, see figure 8. A sudden increase in the peaking rate occurs at 2 s.

The calculated particle source terms using the shown plasma profiles are plotted in figure 3 as a function of the minor radius for the first (black) and the last (yellow) analyzed time point. In the plot on the left side the source rates are given as a change of density at each flux surface per second. The NBI deposition (solid lines) is peaked towards the plasma core which is due to a combination of a volume effect and the plasma density core peaking. As the core density increases during the NBI heating phase also the core particle deposition increases thereby creating a positive feed back loop. The recycling particle deposition falls off exponentially towards the plasma core with both source rates being equal around mid radius. The plasma edge is strongly dominated by the recycling particle fueling. The error is determined from the uncertainty on the used particle confinement time. On the right side the source rates are volume integrated from 0 to ρ. It can be seen that regarding the total particle deposition into the plasma core the NBI dominates up to mid radius.

From the evolution of the carbon concentration in the plasma core (see appendix, figure 9 or [33]) it was found that the main ion density decreases by only ≈2% relative to the electron density in the analyzed time interval. Compared to an absolute change of density of ≈100% during the same time, the effect of impurity accumulation on the deduced particle fluxes in this study is negligible and the results presented in the next chapters are valid for both electrons and main ions.

3.1.2. Anomalous transport. With the time evolution of the plasma density profile and the modeled particle sources at hand, the radial particle fluxes can be computed using equation (2.2) The resulting total electron particle flux is shown in figure 4 at a radius of $\rho = 0.35$ for all included time points. The chosen radial point lies in the region where the

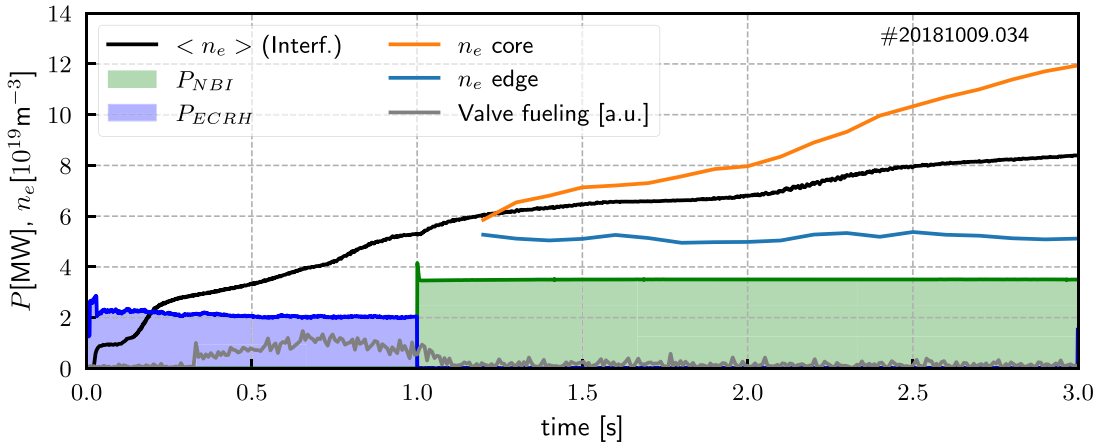

Figure 1. Overview plot of discharge 20181009.034. The plasma is heated by NBI (green) and ECRH (blue). The line integrated electron density measured by the interferometer is shown as a black line and the core and edge electron density measured by the Thomson scattering system is plotted in orange and light blue respectively. The neutral gas inlet flow, fueling the plasma with hydrogen, is plotted in gray.

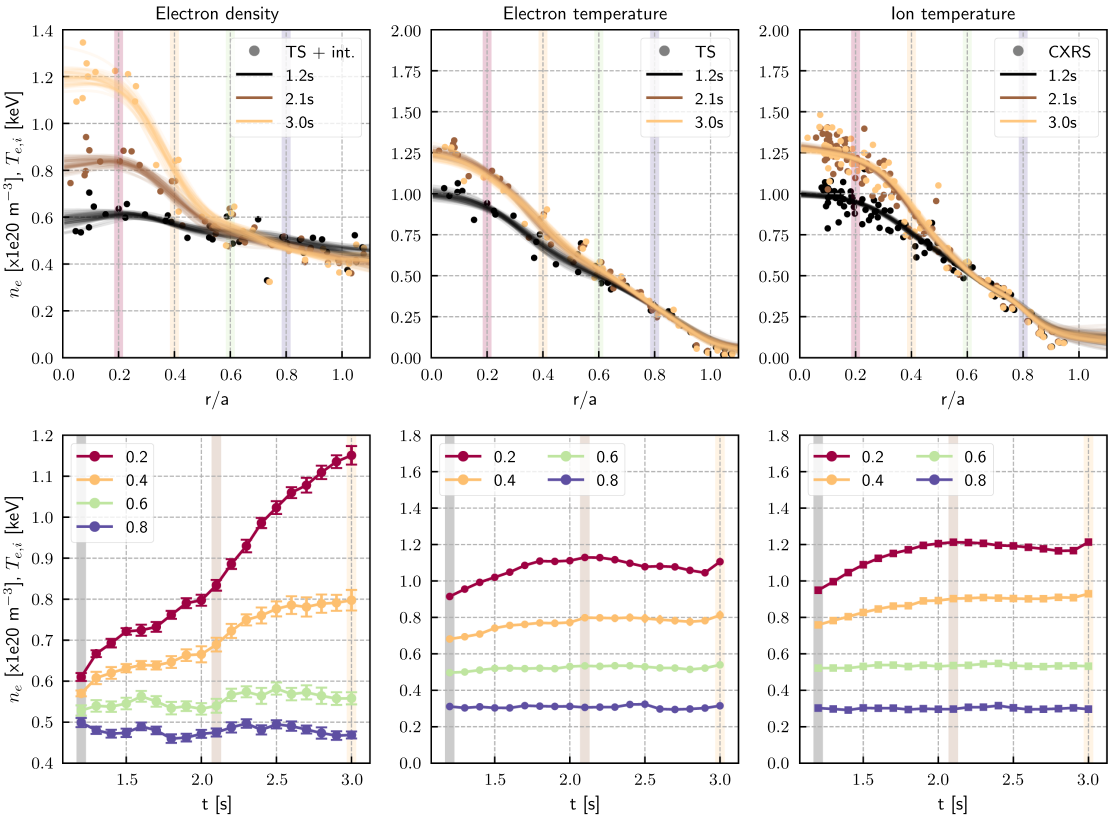

Figure 2. Top row: plasma profiles at three different time points. Close to the beginning of the NBI phase (1.3 s), directly before the peaking accelerates (2.0 s) and at the end of the analyzed time interval (3.0 s). The raw diagnostic data is shown as dots and is fitted using a Monte Carlo sampled local regression method (plotted as lines). The electron density and temperature is measured with the Thomson scattering system (density profile is renormalized using the inferometer system). The ion temperature diagnostic is the CXRS system. Bottom row: plasma profile evolution over time at four chosen normalized radii.

strongest electron density gradient builds up during the discharge. The integrated total particle source rate (blue solid line) slowly increases over the course of the discharge due to a rising NBI particle deposition (blue dashed line) in the plasma core. At 1.2 s and around 2.2 s the total flux (black line) has a clear minimum. The neoclassical contribution (orange line + filled area) to the total flux slowly increases during the analyzed time interval but the variation is insignificant compared to the evolution of the total particle flux. The anomalous flux (green filled area) caused by turbulent processes is assumed to

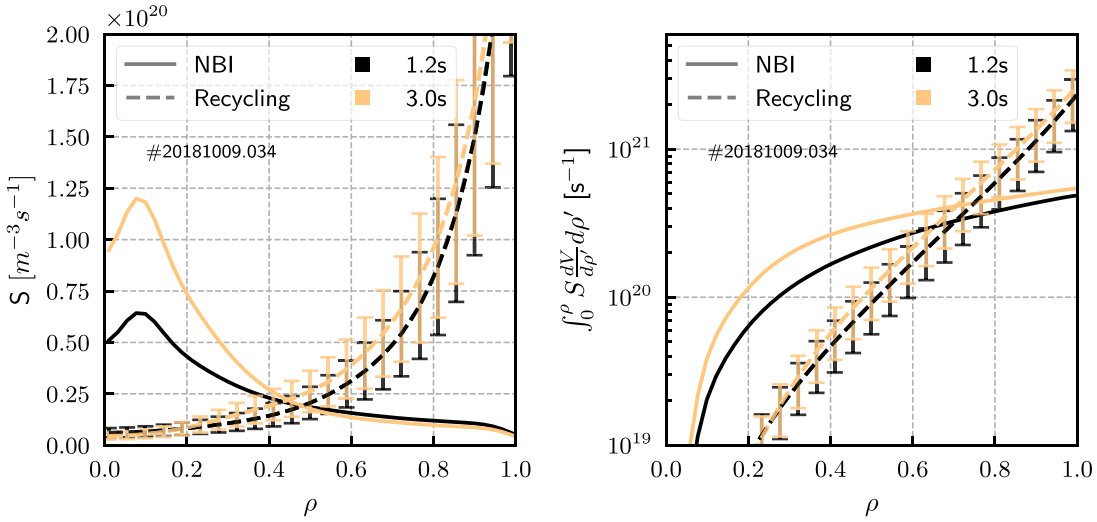

Figure 3. Neutral beam (solid lines) and recycling hydrogen (dashed lines) particle source rates as a function of the normalized minor plasma radius at the beginning (1.2 s, black) and the end (3.0 s, yellow) of the analyzed time interval. Left: the local rates in $m^{-3}s^{-1}$. Right: the volume integrated rates in s^{-1}.

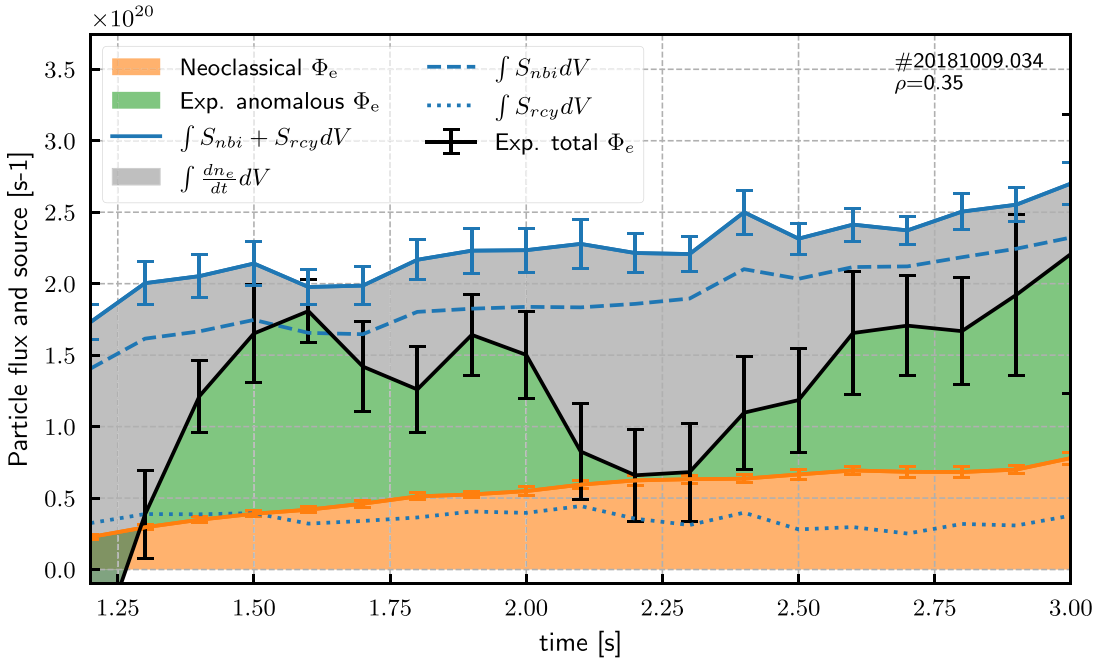

Figure 4. Particle fluxes and integrated source rates at $r/a = 0.35$. The total experimental electron flux (black line) is computed from the total particle source rate (blue solid line) and the change of particle content inside $r/a = 0.35$ (filled gray area) using equation (2.2). The anomalous flux contribution (filled green area) is calculated by subtracting the known neoclassical flux (orange line + filled area).

be the difference between the total flux and the neoclassical flux. At the very first time point and at 2.2 s the total flux is at neoclassical levels.

It is clearly seen that the reduction at 2.2 s, which corresponds to an accelerated increase of the core density, is caused by a change of the anomalous flux and cannot be explained by variation of the neoclassical flux or the particle source terms. Although the reduction of the anomalous flux is only seen transiently, the sudden change seen at 2.2 s poses the question of whether it should be expected from the changes in the electron density and its gradient or whether a more fundamental change of the turbulence character occurs. Additionally, one has to note that the anomalous flux density between 2.5 s and 2.8 s is at a similar level as from 1.4 s to 1.9 s even though the electron density and density gradient have changed significantly (see figure 2). Exploiting the non steady state conditions of the plasma enables the computation of particle transport coefficients using equation (2.4).

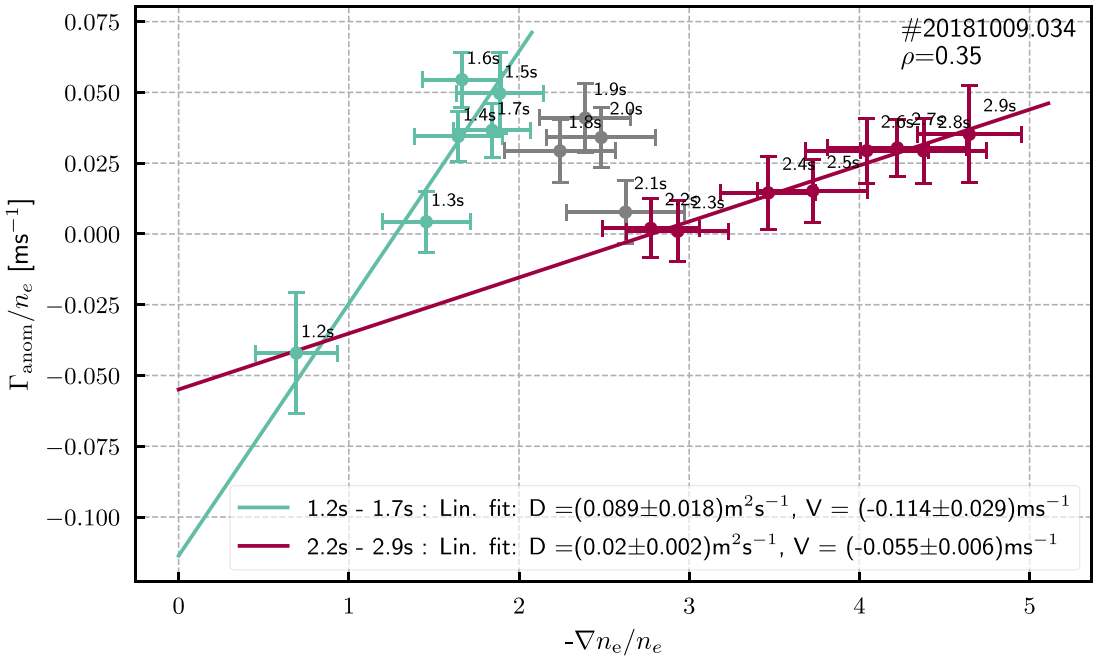

Figure 5. The anomalous flux density divided by the electron density as a function of the profile gradient divided by the density at $r/a = 0.35$ for each analyzed time point in the interval 1.2–3.0 s. Orthogonal regression fits are performed on the data points from 1.2 s to 1.7 s and from 2.2s to 2.9 s yielding the anomalous transport coefficients D_A and V_A. The gray data points are interpreted as a transition phase stretching from 1.8 s to 2.1 s.

In figure 5 the anomalous flux density divided by the electron density is plotted as a function of the normalized density gradient for each analyzed time point at $r/a = 0.35$. If an evolving plasma phase can be described by a set of constant anomalous diffusion (D_A) and convection (V_A) coefficients, there is a linear dependence between the plotted quantities with D_A being the slope and V_A the y-intercept of a linear regression. In the analyzed time interval two phases with strongly correlated data points can be identified. The first phase from 1.2 s to 1.7 s (blue data points) is followed by a 0.4s long transition phase from 1.8 s to 2.1 s (gray data points) leading to a second phase from 2.2 s to 2.9 s (red data points). A linear regression for each of the two high correlation phases yields the anomalous transport coefficients and the results are printed in the figure legend. As the data points have uncertainties in x and y, an orthogonal distance regression is performed which takes both errors into account. According to the fit, the anomalous diffusive transport at the shown radius is significantly reduced in the entire second phase compared to the first phase. In both phases an anomalous convective inward pinch exists which is reduced after the transition.

While a linear response of the turbulent transport flux on changes of densities and density gradients over such a wide range is not necessarily expected, the used diffusion convection model is the simplest empirical parametrization for describing the evolution of these two plasma phases. A similar behavior, though at different plasma parameters, was seen at JET where, over a range of $\frac{\nabla n}{n}$ of 1, a linear response of the total particle flux was measured. The fitted transport coefficients were in agreement with measurements based on non-perturbative techniques [20]. For W7-X these measurements have not yet been performed and will be done in the future.

The same kind of fits can be performed at several radii to obtain a radial profile of D_A and V_A which is shown in figure 6. In the top plot the resulting anomalous D_A and V_A profiles are plotted from $r/a = 0.2$ to 0.5 which is the region where the strongest gradients build up and is thereby the region of interest for the transport analysis. At smaller radii the uncertainty on the density profile gradients pose a limit on the transport information which can be inferred. At radii further out the density profile does not strongly evolve in the analyzed time interval, the gradients are small and the uncertainty on the recycling source is high, which is why the transport coefficients could not be determined in that region. It can be seen that the anomalous diffusion coefficient (green solid line) is significantly reduced in the second phase (red solid line) of the discharge. In both phases the anomalous convection coefficient (green and red dotted lines) is negative which means that the convective flux contribution is directed inwards. Consequently, if the anomalous transport is dominant, the density profile has or evolves towards a slightly or strongly peaked shape depending on the ratio of V_A to D_A which is shown in the bottom plot of figure 6. The neoclassical transport coefficients are included in the plotted V/D ratio. A more negative value leads to the build up of larger negative density gradients in that region. Before and after the transition a clear negative ratio is determined from $r/a = 0.25$ to

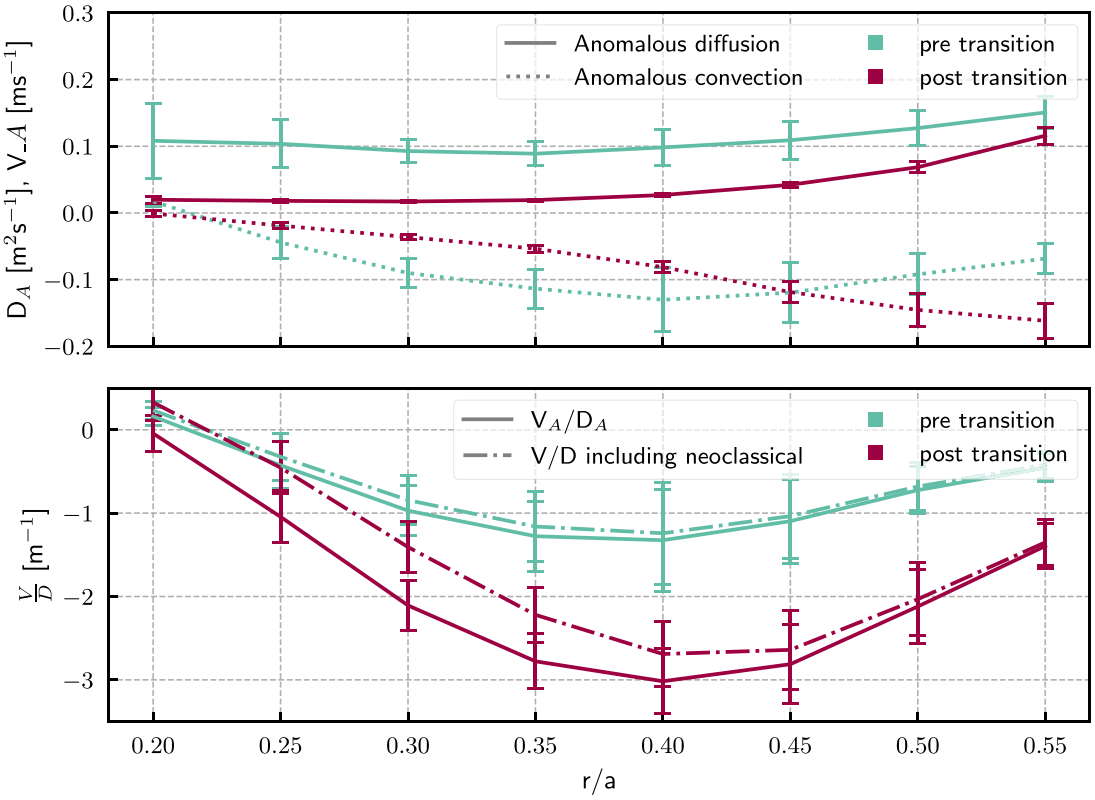

Figure 6. Top: experimentally determined anomalous diffusion (solid lines) and convection (dashed-dotted lines) coefficients as a function of the normalized minor plasma radius *r/a* (only from 0.2 to 0.5) in two plasma phases. The pre transition phase (blue) is from 1.2 s to 1.7 s and the post transition phase (red) from 2.2 s to 3.0 s. The transition is defined as a clear change in transport as already seen in figure. Bottom: the total (anomalous + neoclassical + classical) ratio V/D as a dashed dotted line and the anomalous V/D as a solid line.

0.5 which agrees with the observed density gradients in that region. Over the whole analyzed radial range the V/D ratio becomes more strongly negative during the transition which explains the accelerated density peaking directly after. The transition is caused entirely by a sudden change of the anomalous transport as the small change in neoclassical transport over the NBI phase is gradual and small. It is possible that the anomalous transport also changes in the outer half of the plasma, however, due to the larger error on the recycling fluxes it is not possible to quantify it conclusively here. Planned upgrades of the diagnostic capabilities of measuring recycling neutral densities in the plasma will help in clarifying this point.

3.2. *Particle flux analysis—multiple discharges*

The analysis shown in detail in the last section is repeated for 3 more discharges which exhibit a strong density peaking (#20181009.016, #20181009.021, #20181009.043). In all discharges the purely NBI heated phase is analyzed. The experimentally determined anomalous electron flux density divided by the electron density is plotted as a function of the normalized electron density gradient in the top of figure 7 at $r/a = 0.35$.

It is clearly visible that the discharges #.021 (orange stars) and #.043 (red squares) behave very similarly to the previously in detail analyzed discharge #.034 (green triangles). All three of them show a sudden change of anomalous flux per density when crossing a critical normalized density gradient of $-a\frac{\nabla n_e}{n_e} \approx 1.1$. The transition consistently takes less than 300 ms (all data points are evenly spaced in time with a 0.1s resolution). Analogous to figure 5 the anomalous transport coefficients are deduced from a linear regression fit before and after the transition for each discharge. The resulting V_A/D_A ratios are shown in the bottom plot of figure 7. The error bar in x corresponds to the range in $a\frac{\nabla n_e}{n_e}$ covered by the data used for the regression. An unambiguous transition to a significantly more negative V_A/D_A ratio is seen in all three discharges (around $r/a = 0.35$) when crossing the critical normalized gradient. The data points from #.021, #.034 and #.043 were combined to calculate the average anomalous transport coefficients (top plot: blue and black line). The resulting, 'multi discharge' V_A/D_A (blue and black dots) ratio is shown in the bottom plot. Although the V/D ratios in the discharges are within error bars of each other, it should be noted that the individual V and D values vary slightly between discharges.

It can be seen that during the pure NBI phase in discharge #.043 normalized density gradients $\geqslant 2.5$ are reached which is beyond the range included in the linear regression. These additional data points do not follow the same set of transport coefficients, but start to drop below the flux that would be predicted.

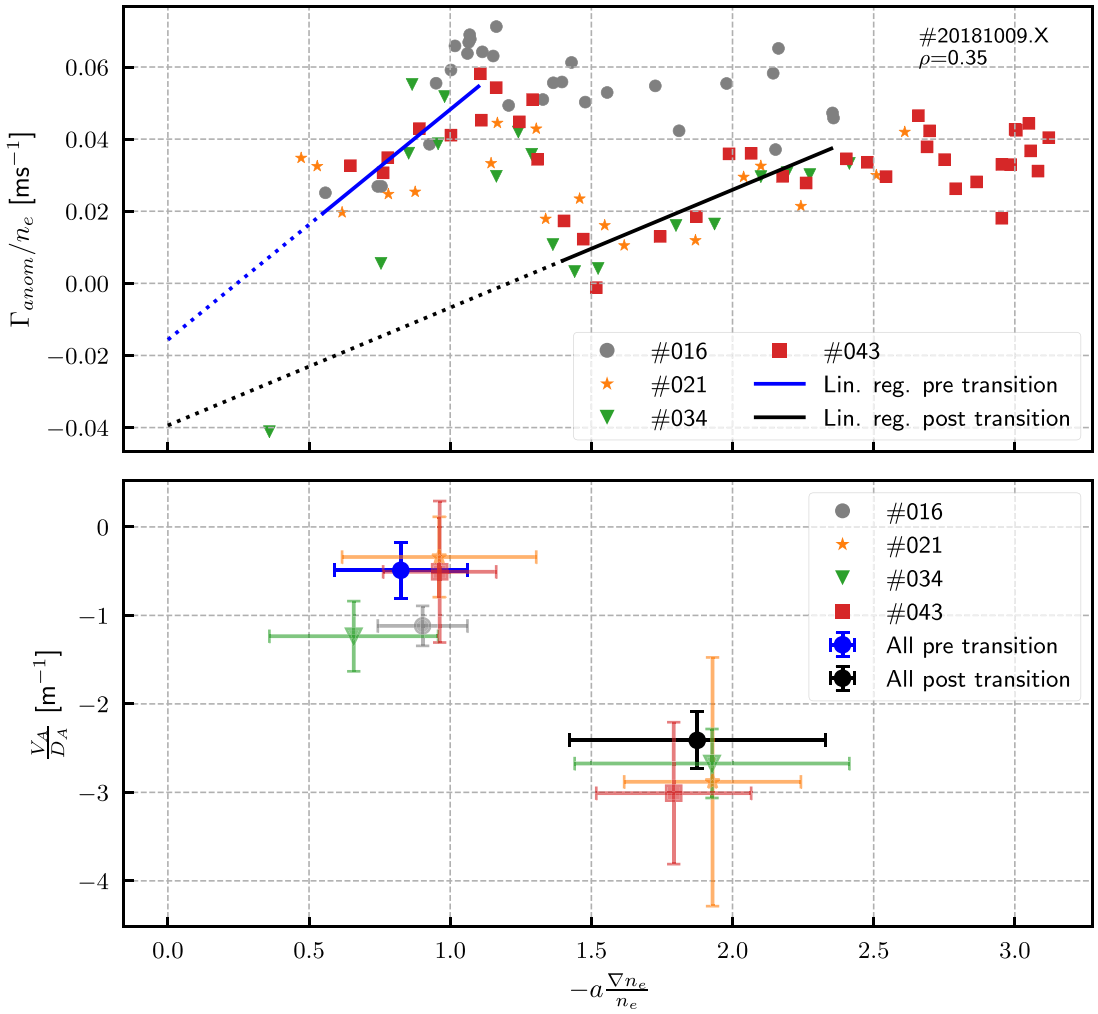

Figure 7. Top: the anomalous electron flux density divided by the electron density as a function of the normalized electron density gradient at a minor radius of $r/a = 0.35$. The evolution of four NBI heated discharges exhibiting peaked density profiles (red, orange, green, gray) is plotted. The data of three of the discharges (#21, #34, #43) is used to perform a linear regression in two different phases indicating the anomalous transport properties during these (blue and black line). Bottom: the ratio $\frac{V}{D}$ of the anomalous transport coefficients in shown regions of the normalized density gradient length. The coefficients are computed from the top plot data points at the shown gradients. The error bar on the y-axis is the uncertainty from the fit and the error bar on the x-axis represents the range the fit was performed on.

As only this one discharge of this duration was available, no clear conclusion can be drawn.

The discharge #.016 (gray dots) behaves differently from the others as it evolves towards higher gradients without a sharp drop of the anomalous flux. It takes 500 ms longer to reach the normalized density gradient where the other discharges show the transition. This is consistent with the NBI phase beginning at a lower line integrated plasma density. Identical to the other discharges, it was possible to fit anomalous transport coefficients in the first phase and the computed V/D value is in the same range as in the other discharges. In the second phase of the discharge, after crossing the critical normalized density gradient, no clear interpretation emerged from the data. When including the same range of points as in the other discharges even a negative diffusion coefficient is determined by the regression which is not physical and simply means that the transport dynamics in that phase cannot be properly described by a single set of D and V coefficients. While dividing the phase into smaller time windows may restore a sensible fit of transport coefficients it then becomes questionable to rely on only very few data points. A noticeable difference to the other analyzed discharges is that in discharge #.016 the ion and electron temperatures at each time point and from $r/a = 0.0$ to 0.8 are both 10%–15% higher. Experimentally, to describe consistent trends more data points are needed.

4. Discussion

Information on plasma particle fluxes in purely neutral beam heated plasma phases could be accessed experimentally by

performing a full particle balance study, requiring knowledge about all particle source terms and the time evolution of the density profile. By exploiting the evolving plasma density it was possible to fit anomalous diffusion and convection coefficients in the high gradient region. While inside mid radius uncertainties on the radial and time derivative of the plasma density proved to be the main source of error, outside mid radius the uncertainty on the recycling particle source became dominant. Generally, the time scatter of the measured density profile prohibited a finer time resolution than 0.1 s in the study. The radial region from $r/a = 0.2$ to 0.5 was found to be of main interest as in this region significantly stronger density gradients build up compared to the outer half of the plasma radius. It was shown through modeling that up to $r/a \approx 0.5$ the accumulated particle fueling is dominated by the NBI and further out by recycling. A strong, transient acceleration of core density peaking after a certain onset time, seen in several discharges, was determined to correspond to a reduction of the anomalous particle flux which happened consistently when crossing a critical normalized density gradient. When parameterized with an anomalous diffusion and convection coefficient, the transient reduction of flux is consistent with a non transient transition to a transport regime with reduced anomalous diffusion and modified convection that remains for the rest of the NBI phase. In all phases the convection coefficient was negative, indicating an inward directed anomalous flux contribution. A consistent change of the V/D ratio to a more negative value when crossing a critical normalized density gradient could be shown.

As the analyzed plasmas do not reach steady state conditions before transitioning, it is possible that the rising density gradient reaches a critical value which in itself stabilizes a turbulent mode and causes the sudden transport change. However, from the used data set, this presumption cannot be proven or disproven as simultaneously the absolute density, the electron and ion temperature profiles as well as the radial electric field evolve. Accordingly, to draw further conclusions experimentally, a wide range of plasma parameters in pure NBI discharges should be covered. Additionally, the option of particle transport studies in ECR heated discharges using NBI blips as density perturbations should be considered.

While it is accepted and shown experimentally that the ion heat transport at W7-X due to ITG modes is reduced by steep density gradients there is no complete theoretical study explaining the presented sudden change of particle transport in these NBI plasmas. Calculations with predictive theory codes for the shown plasma conditions will be needed for a thorough understanding of the turbulent transport dynamics at play. The presented study could then be used for a quantitative comparison with predictions.

Acknowledgment

This work has been carried out within the framework of the EUROfusion Consortium, funded by the European Union via the Euratom Research and Training Programme (Grant Agreement No 101052200 - EUROfusion). Views and opinions expressed are however those of the author(s) only and do not necessarily reflect those of the European Union or the European Commission. Neither the European Union nor the European Commission can be held responsible for them.

Appendix

A.1. Profile gradients and time derivatives—#20181009.034

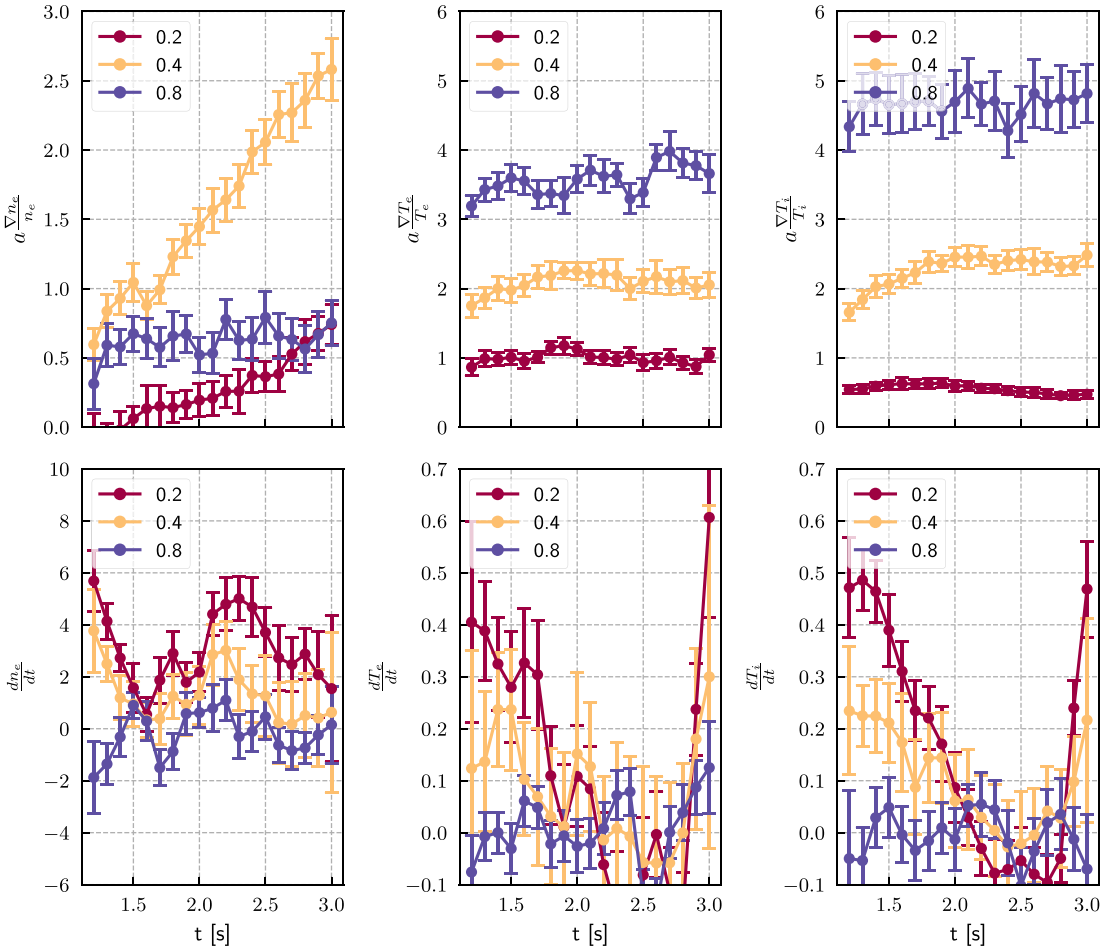

Figure 8. Discharge 20181009.034; top row: radial, normalized gradients of the electron density, the electron temperature and the ion temperature at $r/a = 0.2$ (red), 0.4 (yellow) and 0.8 (blue). Bottom row: time derivatives of the electron density, the electron temperature and the ion temperature at $r/a = 0.2$ (red), 0.4 (yellow) and 0.8 (blue).

A.2. Carbon density profiles - #20181009.034

The carbon density starts peaking in the plasma core after 1 s of NBI. The density profiles measured with the CXRS system are shown in figure 9 and taken from [33].

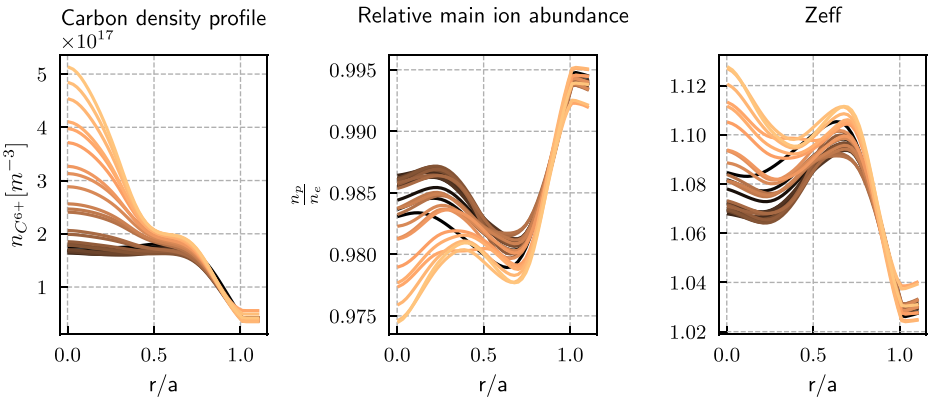

Figure 9. Discharge 20181009.034; left: carbon density from 1.2 s to 3.0 s. Mid: Main ion density divided by electron density in same time interval if assuming that carbon is the dominant impurity. Right: the resulting Z_{eff} profile.

A.3. Comparison of recycling model to EMC3-EIRENE and spectroscopy data

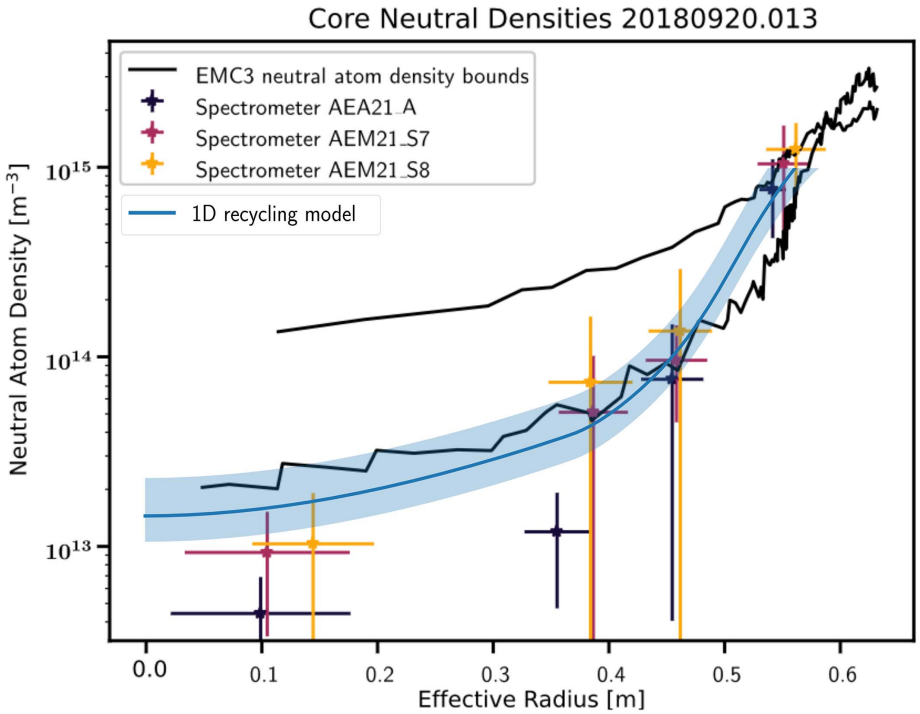

Figure 10. Result of implemented 1D CX diffusion model is shown in blue. Error range is determined from uncertainty in particle confinement time $\tau_p = (0.27 \pm 0.1)$s. The shown scattered data points represent experimental estimations of the neutral density from Balmer-α measurements. The two black lines are the with EMC3 modeled poloidally averaged neutral densities at two different toroidal locations. Reproduced from [26].

ORCID iDs

S. Bannmann https://orcid.org/0000-0003-0772-9278
P.Zs. Poloskei https://orcid.org/0000-0001-7781-5599
A. Pavone https://orcid.org/0000-0003-2398-966X
S. Kwak https://orcid.org/0000-0001-7874-7575
S. Lazerson https://orcid.org/0000-0001-8002-0121
D. Hartmann https://orcid.org/0000-0002-3511-6500
R.C. Wolf https://orcid.org/0000-0002-2606-5289

References

[1] Wolf R.C., Beidler C.D., Dinklage A., Helander P., Laqua H.P., Schauer F., Sunn Pedersen T. and Warmer F. 2016 Wendelstein 7-X program—demonstration of a stellarator option for fusion energy *IEEE Trans. Plasma Sci.* **44** 1466–71
[2] Wolf R. *et al* 2017 Major results from the first plasma campaign of the Wendelstein 7-X stellarator *Nucl. Fusion* **57** 102020
[3] Beidler C.D. *et al* (the W7-X Team) 2021 Demonstration of reduced neoclassical energy transport in Wendelstein 7-X *Nature* **596** 221–6
[4] Beurskens M. *et al* (the W7-X Team) 2021 Ion temperature clamping in Wendelstein 7-X electron cyclotron heated plasmas *Nucl. Fusion* **61** 116072
[5] Carralero D. *et al* (the Wendelstein 7-X Team) 2021 An experimental characterization of core turbulence regimes in Wendelstein 7-X *Nucl. Fusion* **61** 096015
[6] Bozhenkov S. *et al* (W7-X Team) 2020 High-performance plasmas after pellet injections in Wendelstein 7-X *Nucl. Fusion* **60** 066011
[7] Klinger T. *et al* 2019 Overview of first Wendelstein 7-X high-performance operation *Nucl. Fusion* **59** 112004
[8] Romba T., Reimold F., Jaspers R., Ford O., Vanó L. and Klinger T. (the W7-X Team) 2023 Suppression of anomalous impurity transport in NBI-heated W7-X plasmas *Nucl. Fusion* **63** 076023
[9] Maassberg H. *et al* 1993 Transport in stellarators *Plasma Phys. Control. Fusion* **35** B319
[10] Beidler C.D. *et al* 2018 (Expected difficulties with) density-profile control in W7-X high-performance plasmas *Plasma Phys. Control. Fusion* **60** 105008
[11] Thienpondt H. *et al* (The Wendelstein 7-X Team) 2023 Prevention of core particle depletion in stellarators by turbulence *Phys. Rev. Res.* **5** L022053
[12] Helander P. and Zocco A. 2018 Quasilinear particle transport from gyrokinetic instabilities in general magnetic geometry *Plasma Phys. Control. Fusion* **60** 084006
[13] Chaudhary N., Hirsch M., Andreeva T., Geiger J., Hoefel U., Rahbarnia K., Wurden G.A. and Wolf R.C. (the W7-X Team) 2023 Radial localization of electron temperature pedestal and ELM-like events using ECE measurements at Wendelstein 7-X *EPJ Web Conf.* **277** 03004
[14] Koponen J., Geist T., Stroth U., Fiedler S., Hartfuss H.J., Heinrich O., Walter H. and Dumbrajs O. (ECH Group, W7-AS Team) 2000 Perturbative particle transport studies in the W7-AS stellarator *Nucl. Fusion* **40** 365
[15] Stroth U., Geist T., Koponen J.P.T., Hartfuß H.J. and Zeiler P. (ECRH and W7-AS Team) 1999 Evidence for convective inward particle transport in a stellarator *Phys. Rev. Lett.* **82** 928–31
[16] Takenaga H. *et al* 1995 Evaluation of radial particle flux profile based on atomic hydrogen density measurements using laser induced fluorescence and emission at halpha *Nucl. Fusion* **35** 107
[17] Tanaka K. *et al* 2010 Particle transport of LHD *Fusion Sci. Technol.* **58** 70–90
[18] Angioni C., Peeters A.G., Pereverzev G.V., Ryter F. and Tardini G. (ASDEX Upgrade Team) 2003 Density peaking, anomalous pinch and collisionality in tokamak plasmas *Phys. Rev. Lett.* **90** 205003
[19] Garbet X., Garzotti L., Mantica P., Nordman H., Valovic M., Weisen H. and Angioni C. 2003 Turbulent particle transport in magnetized plasmas *Phys. Rev. Lett.* **91** 035001
[20] O'Rourke J., Gowers C., Kramer G.J., Morgan P.D., Simonini R. and Sips A.C.C. 1993 Measurements of the electron source distribution and particle transport coefficients inJET *Plasma Phys. Control. Fusion* **35** 585
[21] Coppi B. and Sharky N. 1981 Model for particle transport in high-density plasmas *Nucl. Fusion* **21** 1363
[22] McNeely P. *et al* 2013 Current status of the neutral beam heating system of W7-X *Fusion Eng. Des.* **88** 1034–7
[23] Lazerson S.A. *et al* (the W7-X Team) 2021 First neutral beam experiments on Wendelstein 7-X *Nucl. Fusion* **61** 096008
[24] Bannmann S. *et al* (the W7-X-Team) 2023 Fast forward modeling of neutral beam injection and halo formation including full Balmer-α emission prediction at W7-X *J. Instrum.* **18** 10029
[25] Kremeyer T. *et al* (the W7-X Team) 2022 Analysis of hydrogen fueling, recycling and confinement at Wendelstein 7-X via a single-reservoir particle balance *Nucl. Fusion* **62** 036023
[26] Winters V.R. *et al* (the W7-X Team) 2021 EMC3-EIRENE simulation of first wall recycling fluxes in W7-X with relation to H-Alpha measurements *Plasma Phys. Control. Fusion* **63** 045016
[27] Pasch E., Beurskens M.N.A., Bozhenkov S.A., Fuchert G., Knauer J. and Wolf R.C. (W7-X Team) 2016 The Thomson scattering system at Wendelstein 7-X *Rev. Sci. Instrum.* **87** 11E729
[28] Bozhenkov S. *et al* 2017 The Thomson scattering diagnostic at Wendelstein 7-X and its performance in the first operation phase *J. Instrum.* **12** 10004
[29] Ford O.P. *et al* 2020 Charge exchange recombination spectroscopy at Wendelstein 7-X *Rev. Sci. Instrum.* **91** 023507
[30] Pablant N. *et al* (the W7-X Team) 2020 Investigation of the neoclassical ambipolar electric field in ion-root plasmas on W7-X *Nucl. Fusion* **60** 036021
[31] Alonso J. *et al* (the W7-X Team) 2022 Plasma flow measurements based on charge exchange recombination spectroscopy in the Wendelstein 7-X stellarator *Nucl. Fusion* **62** 106005
[32] Smith H. 2023 Neotransp (available at: https://gitlab.mpcdf.mpg.de/smithh/neotransp)
[33] Romba T. 2021 Validation of the W7-X CXRS for impurity density profiles *Master's Thesis* (available at: https://pure.tue.nl/ws/portalfiles/portal/194477468/1410342_Romba_T._MSc_thesis_Thesis_MAP_MNF.pdf)
[34] Vanó L. 2022 Carbon content and transport investigations on Wendelstein 7-X with charge exchange recombination spectroscopy *PhD Thesis* https://doi.org/10.14279/depositonce-16591
[35] Kwak S. *et al* 2021 Bayesian inference of spatially resolved Z_{eff} profiles from line integrated bremsstrahlung spectra *Rev. Sci. Instrum.* **92** 043505